Relationship between movement types of shallow landslide and topographical and geological conditions in Da Nang City, central Vietnam

Yamaguchi Akari, Sato Go（Tokyo City Univ.）, Nguyen Van Thang, The Viet Tran (Thuyloi Univ.)

In recent years, the frequency and magnitude of soil disasters in Vietnam have increased owing to extreme weather events associated with global warming. For instance, in the southwestern region of Da Nang City, central Vietnam, many landslides were triggered by the heavy rainfall caused by Typhoon Molave in October 2020. Yamaguchi et al. (2025) created a landslide distribution map for the study area and found that the frequency of landslides varied across different geological settings. However, understanding only the distribution characteristics of landslides is insufficient for elucidating the movement processes of landslide debris, including flow paths and deposition areas. Therefore, in this study, the geomorphic interpretation of satellite imagery was conducted with reference to Hao Ma et al. (2024). Landslide movement types are classified by distinguishing between the sources of landslides and their deposition areas. Furthermore, the relationships between landslide movement types and geological and topographical characteristics are discussed.

Keywords: Remote sensing, Landslide distribution map, Geomorphic analysis, Da Nang City

Study Area

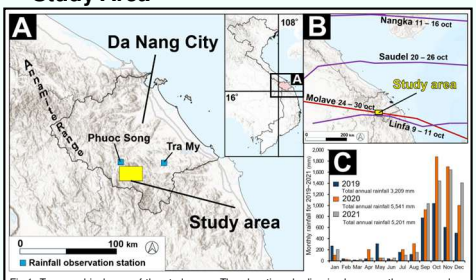

Fig.1. Topographical map of the study area. The elevation shading is shown on the map, and the elevation map is also displayed. The base map was created using the 30-m Digital Surface Model (DSM) from the Japanese Advanced Land Observing Satellite.

The study area is located in the southwestern part of Da Nang City within the mountainous region that forms part of the Annamite Range **A**. In October 2020, four cyclones, Linfa, Nangka, Saudel, and Molave, hit central Vietnam**B**. **Typhoon Molave** brought heavy rainfall to Da Nang City in central Vietnam, leading to widespread landslides in the region's mountainous areas. In the city's Tra My District, total rainfall from October 2020 reached **1,800 mm C**.

Classification of landslide movement types

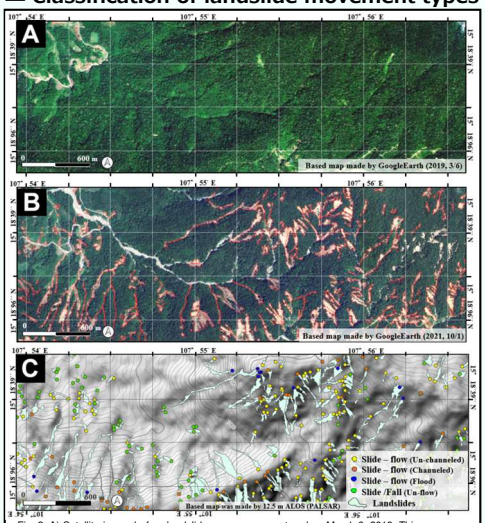

Fig. 2. A) Satellite image before landslide occurrence, captured on March 6, 2019. This map was made using Google Earth satellite imagery. B) Satellite image after landslide occurrence, captured on October 1, 2021. This map was made using Google Earth satellite imagery. C) Distribution of landslides classified by movement type. This map was made from the 30-m resolution Digital Surface Model (DSM) of ALOS (PALSAR).

Geomorphic interpretation was performed using **satellite images (Google Earth)** to classify landslides according to the movement type. Figure 2 (A–C) shows satellite images taken before and after the landslides and the distribution of landslides classified by movement type. The polygons delineating the landslide areas were not separated into **landslide sources** and **deposition areas**. Instead, both landforms were treated together as a single landslide area (Fig. 2B). These points were also identified as landslide sources (Fig. 2C). All landslides were **manually classified** according to movement type.

Table 1. Typical characteristics for identifying landslide movement types

Movement types of landslide	Description
Slide-flow(Non-channeled)	The landslide mass moves without being constrained by valley morphology.
Slide-flow (Channeled)	The landslide mass moves while constrained by the valleys. Channels' morphology.
Slide-flow (Bed erosion)	The landslide mass becomes fluidized and travels downslope while eroding the slope bed.
Slide・Fall (Non-flow)	No apparent fluidization is observed in the landslide mass. This type primarily corresponds to small-scale slides or rockfalls.

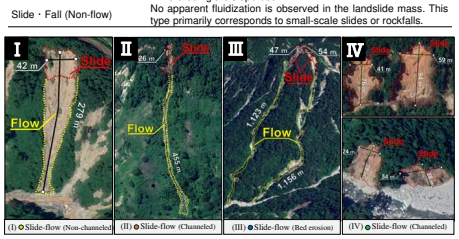

Fig.3. Typical identification characteristics of landslide movement types reflected in satellite imagery.

Following the classification of Hao Ma et al. (2024), they were categorized into four types: **Slide-flow (Non-channeled)** I as shown in, **Slide-flow (Channeled)** in II, **Slide-flow (Bed erosion)** III in, and **Slide/fall (Non-flow)**IV in As shown in Table 2, the landslides were classified according to the **landslide topography**, occurrence of **flow**, presence of **channels**, and extent of the **deposition area**.

Distribution of landslides and characteristics of landslide area by Movement types

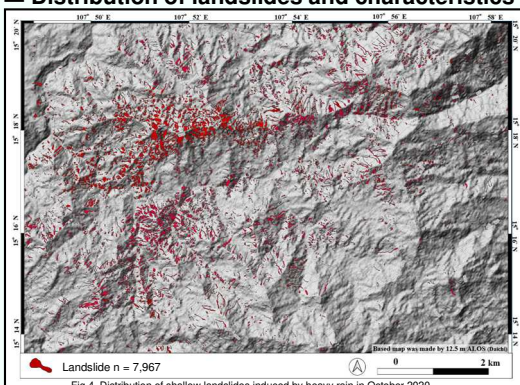

Fig.4. Distribution of shallow landslides induced by heavy rain in October 2020.

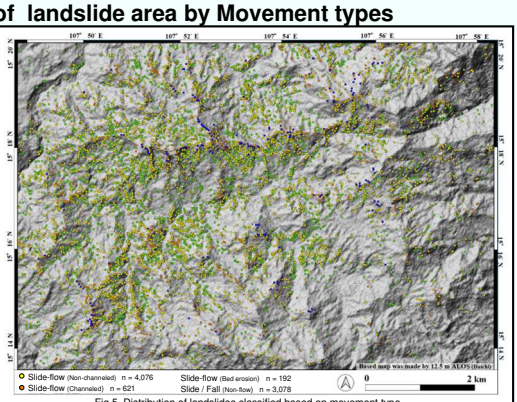

Fig.5. Distribution of landslides classified based on movement type.

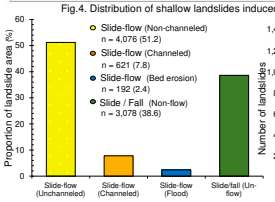

Fig 6 Proportion and number of landslides by movement type

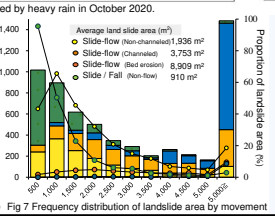

Fig 7 Frequency distribution of landslide area by movement

Figure 4 presents the overall distribution of landslides within the study area, while Figure 5 shows the distribution classified by movement type. As indicated in Figure 6 and 7, **slide-flow (non-channeled) landslides accounted for 51.2% of all cases, representing the most dominant type**. Slide/fall (non-flow) types made up 38.6 %, followed by slide-flow (channeled) at 7.8 %, and slide-flow (bed erosion) at 2.4 %. Regarding the average landslide area for each movement type, **slide-flow (bed erosion) landslides had the largest average area at 8,909 m²**, followed by slide-flow (channeled) at 3,754 m², slide-flow (non-channeled) at 1,937 m², and slide/fall (non-flow) at 911 m².

Methods: Relationship between Landslide Movement Types, Topography, and Geology

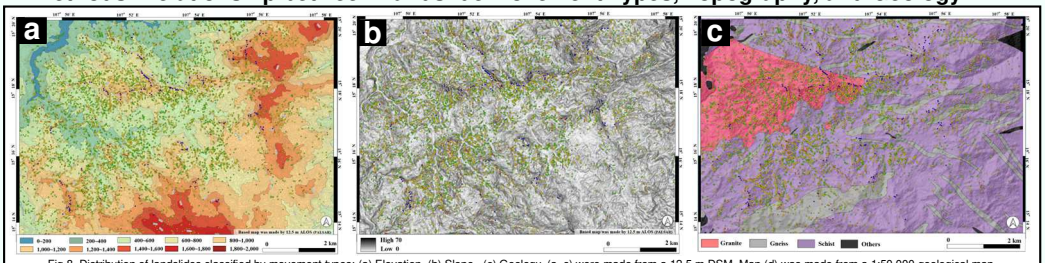

Fig.8. Distribution of landslides classified by movement types: (a) Elevation, (b) Slope, (c) Geology. (a–c) were made from a 12.5 m DSM. Map (d) was made from a 1:50,000 geological map.

Topographic analysis was conducted on landslide source areas to **clarify topography characteristics associated with each movement type**. In this study, elevation and slope angle shown in Fig 8a and 8b were utilized. To examine the **relationship between landslide movement types and geological conditions**, a comparative analysis was performed using three major geological units—granite, gneiss, and schist—as shown in Figure 8c .

Results: Relationship between landslide movement types, topography, and geology

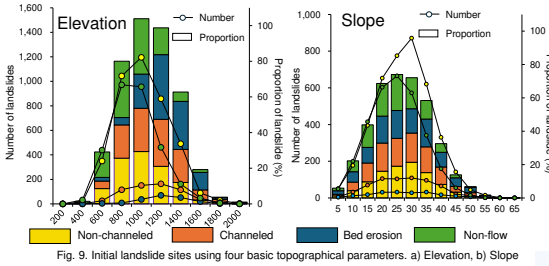

Fig. 9. Initial landslide sites using four basic topographical parameters. a) Elevation, b) Slope

Table 2. Topographic analysis results showing the proportion of landslides by movement types according to elevation classes.

Elevation (m)	0~200	200~400	400~600	600~800	800~1,000	1,000~1,200	1,200~1,400	1,400~1,600	1,600~1,800	1,800~2,000
Non-channeled	0	0.4	8.6	25.6	29.3	21.1	12.0	2.2	0.7	0
Channeled	0	0	4.2	18.7	24.3	26.4	18.5	5.6	1.8	0.5
Bed erosion	0	0	2.1	4.1	19.2	36.3	26.9	9.8	1.0	0.5
Non-flow	0	1.0	14.3	31.6	31.1	15.0	5.3	1.6	0.2	0

Table 3. Topographic analysis results showing the proportion of landslides by movement types according to slope classes.

Slope (°)	0~5	5~10	10~15	15~20	20~25	25~30	30~35	35~40	40~45	45~50	50~55	55~60	60~65
Non-channeled	1.3	4.3	9.7	16.0	19.0	21.4	15.2	8.1	3.5	1.1	0.4	0	0
Channeled	1.0	5.1	11.3	16.9	16.7	17.5	15.4	10.5	3.4	2.1	0.2	0	0
Bed erosion	2.1	6.3	9.4	16.1	16.7	14.6	16.7	8.9	5.2	3.1	1.0	0	0
Non-flow	1.6	6.5	13.5	19.6	21.6	18.6	11.1	5.2	1.8	0.5	0	0	0

Table 4. Average landslide area by movement types for each geological unit.

Landslide types	Granite	Gneiss	Schist
Slide-flow (Non-Channeled)	2,310 m² (49.9 %)	1,606 m² (59.2 %)	1,841 m² (50.5 %)
Slide-flow (Channeled)	4,999 m² (5.8 %)	4,317 m² (11.0 %)	3,264 m² (8.1 %)
Slide-flow (Bed erosion)	9,915 m² (2.7 %)	11,798 m² (1.8 %)	8,102 m² (2.4 %)
Slide/Fall (Non-flow)	1,263 m² (41.6 %)	858 m2 (27.9 %)	758 m² (39.0 %)

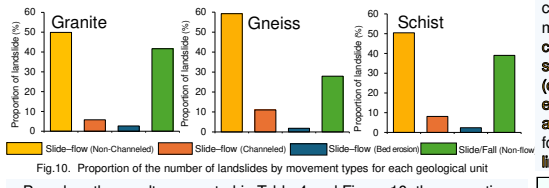

Fig.10. Proportion of the number of landslides by movement types for each geological unit

Based on the results presented in Table 4 and Figure 10, the proportions of landslide occurrences by movement type showed **no significant differences among the three main geological units (granite, gneiss, and schist).** However, **the granite area had a larger average landslide area than the others**, especially for slides and falls (Non-flowing). **A thick weathered zone of decomposed granite characterizes this area. Rainfall infiltration into this layer likely increased pore water pressure at the boundary with the underlying bedrock**, triggering large-scale landslides.

Based on the results presented in Figure 9 and Tables 2 and 3,Slide-flow (non-channeled) landslides were concentrated at elevations of 600–1,000 m on slopes of 20–30° , with many sources located on ridges and middle slopes. Slide-flow (channeled) landslides occurred at 800–1,200 m on slopes of 15–30° , and slide-flow (bed erosion) types at 1,000–1,400 m on slopes of 20–35° , both mostly originating from ridges and middle slopes. Slide/fall (non-flow) landslides were concentrated at 600–1,000 m on slopes of 15–25° , with sources on middle and lower slopes. These results indicate that **slide-flow (non-channeled) landslides tended to occur at lower elevations and middle slopes compared to other flow-type landslides**. In contrast, **slide-flow (channeled) and bed erosion types were more frequent at higher elevations and steep ridge slopes**, suggesting **downslope movement along valley topography.** Slide/fall (non-flow) landslides were typically found on gentler slopes and lower to middle slope positions, **implying limited movement and short runout distances or near-source deposition.**

References

Yamaguchi Akari, Sato Go, The Viet Tran, Nguyen Van Thang, Ozaki Takatsugu (2025). Evaluating Landslide Dimensions and Distribution Across Different Geological Settings in Quang Nam Province Following Typhoon Molave, Proceedings of the 5th ICSCE, Vol 2.

Hao Ma, Fawu Wang (2024). Inventory of shallow landslides triggered by extreme Precipitation in July 2023 in Beijing, China, Scientific Data, Vol 11.

Tran, A.T., Tran, T.T., Pham (2023): Landslide Susceptibility mapping based on the Weights of Evidence model for mountainous areas of Quang Nam province, Vietnam, Hydro-Meteorology, pp. 31-45.

This study was supported by JSPS KAKENHI Grant Numbers JP24K00174 and JP24KK0097.